

Trajectory Optimization of Multirotor Agricultural UAVs

Priyank Pradeep
Department of Aerospace Engineering
Iowa State University
Ames, IA, USA.
ppradeep@iastate.edu

Sang Gyun Park
Optimal Synthesis Inc.
Los Altos, CA, USA.
sang.park@optisyn.com

Peng Wei
Department of Aerospace Engineering
Iowa State University
Ames, IA, USA.
pwei@iastate.edu

Abstract— Multirotor agricultural unmanned aerial vehicles (UAVs) are perceived as one of the key enablers for precision agriculture (PA) in near future. UAVs capture images with much higher resolution compared to satellites and airplanes because of the low altitude remote sensing (≤ 400 ft above ground level in the USA). UAVs also provide better operational and temporal flexibility to react quickly to undesirable weather events. The sensitivity of the image capturing devices (thermal and multispectral) to exhaust gases makes gas powered UAVs practically unusable for PA's scouting or sensing tasks. Therefore, agricultural UAVs are typically electric powered using lithium-polymer (Li-Po) batteries. However, the endurance of Li-Po battery pack imposes severe constraints on the operational time span of an electric UAV during an agricultural mission. Hence, optimal path planning is critical for maximizing farm field area coverage and minimizing operational cost for image acquisition per flight. Our research contribution focuses on the trajectory optimization of multirotor UAVs in multi-phase optimal control framework with field area coverage and energy as two separate performance indexes to be maximized and minimized respectively. The mathematical relationship between the thrust produced and power consumed by a UAV is derived using momentum theory for the climb, cruise, and descent phases. Finally, the two optimal control problems formulated are numerically solved using pseudospectral method for an actual UAV product: DJI Phantom 4.0 quadcopter.

emerging technological field which provides promise for the increase in agricultural productivity by using data on the spatial variability of soil and crop characteristics to optimize the amount and timing of field applications of inputs like seed, fertilizer, and irrigation [3]. Hence, PA is a way to apply the right agricultural treatment in the right place at the right time to increase agricultural productivity. The four stages of PA practice are i) data collection, ii) field variability mapping, iii) decision making, and iv) management practice [4], [5]. It is suggested that remote sensing could be involved in the first three stages of PA practice. In particular, up-to-date imagery acquisition and timely data processing are critical during the process of decision making, thus field variability can be efficiently mapped using remotely sensed imagery [5]. The basic underlying premise of remote sensing applications in PA is that differences in crop growth and soil condition can be detected through variations within the spectral responses [6]. The remote sensing of a farm field can be carried out by using the following three platforms 1) satellite, 2) aircraft, and 3) unmanned aerial vehicle (UAV).

1.2 Motivation

Satellite images and aerial photos collected for PA are limited by revisiting times, weather conditions and/or coarse spatial resolutions [5]. Resolutions measured in meters tend to be good enough for large scale projects in agriculture, resource exploration, and land-use planning, but not for a detail oriented PA tasks [3]. Airplanes present a compromise between satellites and UAVs, providing higher resolution imagery than satellites but also being able to cover much larger areas than UAVs. However, their usage is limited by high operational complexity, costs and lengthy delivery of products. On the other hand, UAVs offer very high spatial resolutions (in centimeters) in real-time at relatively much lower operating costs because of the low altitude remote sensing system [7]. This indicates that UAVs are the ideal platform for mapping and monitoring in PA. The sensitivity of the image capturing devices (thermal and multispectral) to exhaust gases makes gas powered UAVs practically unusable for PA's scouting and sensing tasks [8]. Therefore, agricultural UAVs are typically electric powered using lithium-ion polymer (Li-Po) batteries.

Multirotor UAVs are known for low cost, good maneuverability and vertical take-off and landing (VTOL) capability. This makes them suitable for PA's remote sensing tasks. However, because of the short flight endurance (20-30 min) from Li-Po batteries, UAVs have a smaller field area coverage per flight compared to airplanes. Our research presented in this paper is motivated to increase flight endurance of electric-powered multirotor UAVs. Trajectory optimization is essential in this paper for the maximization of the farm field area coverage per UAV flight given limited battery power. Finally, we used DJI Phantom 4.0 as our specific aircraft example for numerical study because the Phantom series quadcopters are one of the most widely used multirotor UAVs by farmers and agriculture

TABLE OF CONTENTS

1. INTRODUCTION.....	1
2. OPTIMAL CONTROL PROBLEM FORMULATION	2
3. NUMERICAL STUDY	4
4. CONCLUSION	6
REFERENCES	6
BIOGRAPHY	7

1. INTRODUCTION

The world population is expected to cross 9 billion mark by 2050. Studies have shown that global crop production needs to double by 2050 to meet the projected demands from rising population [1]. Agriculture has to produce more food for a growing population with a smaller rural labor force and shrinking farm lands because of the high speed of global urbanization [2]. This challenge can only be solved by boosting crop yields to meet these rising demands [1]. Therefore, more efficient and sustainable crop production methods need to be incorporated in farming.

1.1 Background

Precision Agriculture (PA) is an information-based management of agricultural production systems [3], [4]. PA is an

service professionals for PA in the USA.

2. OPTIMAL CONTROL PROBLEM FORMULATION

2.1 Flight Dynamics of Multirotor UAVs

The lateral path of multirotor UAVs is assumed to be in back-and-forth pattern [9]. In order to minimize the number of turns outside the coverage area and hence field coverage time, the rows are assumed perpendicular to the sweep direction, as shown in Figure 1 [9].

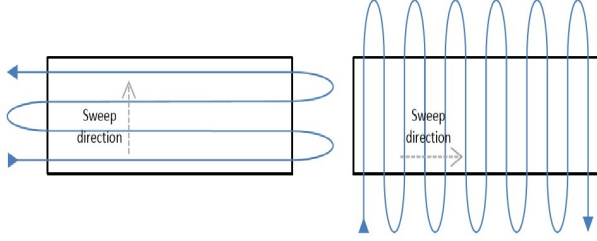


Figure 1. Lateral path of a UAV to minimize the number of turns [9].

In general, multirotor UAVs (quadcopters, hexacopters and octocopters) have more symmetrical i) fuselage shape and ii) location and orientation of rotors with respect to the center of mass than helicopters [10]. Hence, longitudinal and lateral dynamics of multirotor UAVs can be decoupled from one another, given that it has already been done for helicopters by a few researchers [11], [12], [13]. The flight dynamics model used in the current research is based on our research on trajectory optimization of an electric VTOL (eVTOL) vehicle [10]. In a fixed inertial frame of reference, by assuming point mass model with quasi-steady flight, the two dimensional equations of longitudinal dynamics of a multirotor UAV are as follows [10]:

$$\frac{dV_x}{dt} = \frac{T \sin \theta - D \cos \gamma}{m} \quad (1)$$

$$\frac{dV_h}{dt} = \frac{T \cos \theta - D \sin \gamma - mg}{m} \quad (2)$$

$$\frac{dx}{dt} = V_x \quad (3)$$

$$\frac{dh}{dt} = V_h \quad (4)$$

$$T = \sum_{N=1}^N T_i \quad (5)$$

where $[x, h]$ is the position vector (along track distance, altitude) of the center of mass relative to the origin (inertial frame of reference), θ is the tip-path-plane pitch angle, T is the net thrust, D is the net drag, T_i is the thrust produced by the i^{th} rotor, m is the mass, N is the total number of arms or rotors in the multirotor UAV, $[V_x, V_h]$ are the horizontal and vertical components of the true airspeed and g is the acceleration due to gravity. Also, the pitch angle (θ), angle of attack (α) and flight path angle (γ) are related as follows [10]:

$$\alpha = \theta + \gamma \quad (6)$$

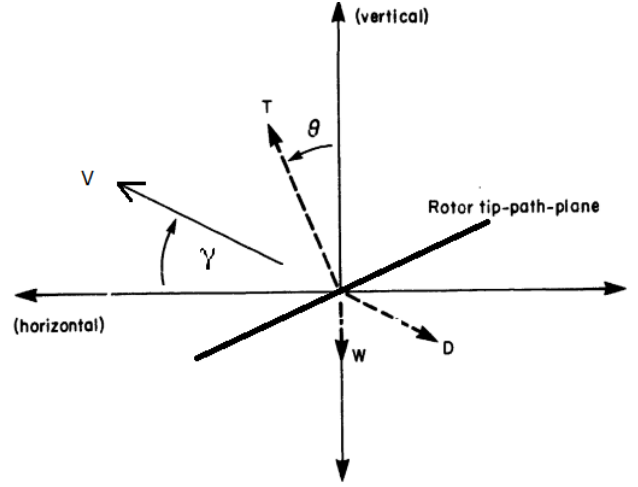


Figure 2. Definition of the vehicle's position, velocity, and forces [13].

2.2 Energy Management

Energy balance equation for a multirotor UAV is given by [12]:

$$\sum_{i=1}^N I_i \omega_i \frac{d\omega_i}{dt} = \sum_{i=1}^N P_i - P_{\text{required}} \quad (7)$$

where P_i is the energy supplied to the i^{th} rotor, P_{required} is the instantaneous power required by the vehicle (to overcome induced drag, profile drag, parasite drag and/or gravity to climb), ω_i is the rotational speed of the i^{th} rotor and I_i is the rotational moment of inertia of the i^{th} rotor. However, based on assumption of quasi-steady flight in the current research:

$$\sum_{i=1}^N P_i = P_{\text{required}} \quad (8)$$

The power supplied by the battery to the ideal i^{th} rotor at time t is given by [14]:

$$P_i(t) = V_i(t) I_i(t) \quad (9)$$

where $V_i(t)$ is the voltage across the motor of the i^{th} rotor and $I_i(t)$ is the current through it [14], [15]. Therefore, equating the total energy supplied by the pack of batteries to the ideal power consumed by all the rotors (N) in total is given by:

$$\sum_{i=1}^N P_i = \sum_{i=1}^N V_i(t) I_i(t) \quad (10)$$

2.3 Momentum Theory in Hover

Using momentum theory [14], [16], [17], the induced velocity (v_h) in hover is given by:

$$v_h = \sqrt{\frac{T_{\text{rotor}}}{2\rho A}} \quad (11)$$

where T_{rotor} is the thrust produced by the rotor, A is the rotor disk area (πR^2), R is the radius of the rotor and ρ is the density of the air.

2.4 Momentum Theory in Forward Flight

Consider a rotorcraft in forward motion at true airspeed V , with angle of attack α between the air-stream and the rotor disk (tip path plane). The solution for induced velocity (v_i) is [14], [16], [17]:

$$v_i = \frac{v_h^2}{\sqrt{(V \cos \alpha)^2 + (V \sin \alpha + v_i)^2}} \quad (12)$$

The thrust produced by the ideal rotor per power input:

$$T_{\text{rotor}} = \frac{P_{\text{rotor}}}{V \sin \alpha + v_i} \quad (13)$$

2.5 Drag Model

Based on the maximum ground speed of UAVs (≤ 100 kts) per Small Unmanned Aircraft Systems (sUAS) Regulations (part 107) in the United States, UAVs operate in $M < 0.3$ flow regime and hence the drag force on the fuselage of the vehicle can be modeled based on the incompressible flow theory. The net drag on the vehicle is assumed to be equivalent to the parasite drag on the fuselage of the vehicle [10]. Therefore, the net drag on the vehicle is calculated as follows [12], [18]:

$$D = \frac{\rho V^2 C_D F}{2} \quad (14)$$

where F is the equivalent flat plate area of the fuselage, V is the true air speed and $C_D = 1$ [12]. The horizontal and vertical components of the drag in fixed inertial frame of reference are as follows [10]:

$$D_x = \frac{\rho V_x^2 C_D F_x}{2} \quad (15)$$

$$D_h = \frac{\rho V_h^2 C_D F_h}{2} \quad (16)$$

where F_x and F_h are the equivalent front and top flat plate area of the fuselage respectively.

2.6 UAV Footprint

The UAV footprint is calculated based on the assumption that camera lens is placed straight down as shown in Fig. 4. The distance between two rows is chosen as a function



Figure 3. Sentera Multispectral Sensor Upgrade for DJI Phantom 4.

of the footprint of the on-board camera on the ground [19]. Based on the width of the image sensor (l), the focal distance of the camera's lens (f) and the height of the camera above the ground (H), it is possible to compute the width L of the camera's footprint as [9]:

$$L = H \frac{l}{f} \quad (17)$$

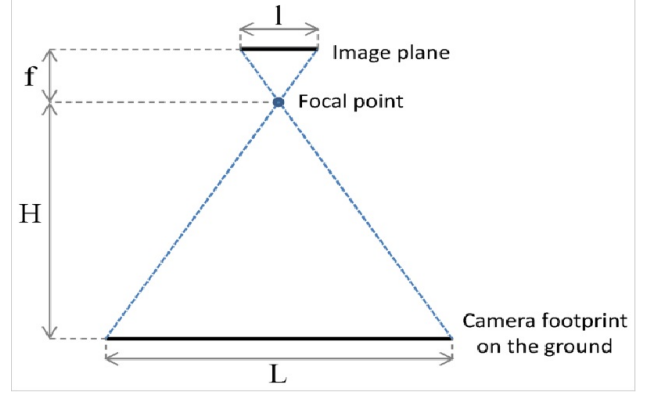


Figure 4. Relationship between l , f , H and L [9].

2.7 Ground Sampling Distance

The Ground Sampling Distance (GSD), is the distance on the ground equivalent to the distance between two consecutive pixel centers on the image [20]. The GSD of digital cameras is calculated as follows [22]:

$$GSD = H \frac{\text{Pixel Size}}{f} \quad (18)$$

where H and f are as defined in Section 2.6. Since most small UAVs fitted with multispectral camera have the capability to collect multispectral imagery at cm-level resolution [21]. Therefore, in the current research variation of the GSD (spatial resolution) of imagery with the altitude of UAV (≤ 400 ft AGL) is ignored. Also, for the commercial multispectral cameras during the low altitude remote sensing the UAV footprint can be computed assuming constant field of view (FOV) of the camera. Consequently, the UAV footprint for a UAV on an agricultural mission is as follows:

$$L = 2H \tan\left(\frac{FOV}{2}\right) \quad (19)$$

2.8 Performance Indexes in Lagrange Form

The objectives of the current research are to study the following of multirotor UAVs:

- i) maximum field area coverage trajectory.
- ii) minimum energy trajectory.

However, it should be noted that the maximum field area coverage trajectory optimization problem is not the same as the maximum range optimal control problem, as the former is solved for a fixed flight time where as the later is solved for a given state of charge of the battery. The performance index (Lagrange form) of the multiphase optimal control problem to maximize field area coverage by a multirotor UAV on an

agricultural mission is as follows:

$$J_{area} = \sum_{phase=1}^3 \int_{t_0^{phase}}^{t_f^{phase}} \frac{dA}{dt} dt \quad (20)$$

where phase is the vertical flight phase (phase = 1 for climb, phase = 2 for cruise and phase = 3 for descent(arrival)), N is the number of rotors/arms and $\frac{dA}{dt}$ is the instantaneous area coverage rate by the UAV.

The differential area coverage dA can be written as:

$$dA = dxL \quad (21)$$

where dx is the differential along-track distance and L is the width of camera's footprint. Hence, the area coverage rate can be written as:

$$\frac{dA}{dt} = \frac{dx}{dt} L \quad (22)$$

$$\frac{dA}{dt} = V_x L \quad (23)$$

By using the equation for UAV footprint:

$$\frac{dA}{dt} = 2V_x H \tan\left(\frac{FOV}{2}\right) \quad (24)$$

The above equation implies that area coverage rate depends on the product of the horizontal component of the true air-speed (V_x) and height of the camera above the ground (H). This can be further approximated as product of V_x and current altitude (h) of the multicopter UAV ($H \approx h$ i.e. the ground at mean sea level). Hence, the performance index is defined as:

$$J_{area} = \sum_{phase=1}^3 \int_{t_0^{phase}}^{t_f^{phase}} 2V_x h \tan\left(\frac{FOV}{2}\right) dt \quad (25)$$

$$J_{area} = \sum_{phase=1}^3 2 \tan\left(\frac{FOV}{2}\right) \int_{t_0^{phase}}^{t_f^{phase}} V_x h dt \quad (26)$$

The performance index (Lagrange form) of the multiphase optimal control problem to minimize energy consumed by a multicopter UAV on an agricultural mission with a constant cruise ground speed and for a fixed duration of flight is as follows:

$$J_{energy} = \sum_{phase=1}^3 \int_{t_0^{phase}}^{t_f^{phase}} \sum_{i=1}^N P_i dt \quad (27)$$

$$J_{energy} = \sum_{phase=1}^3 \int_{t_0^{phase}}^{t_f^{phase}} P_{required} dt \quad (28)$$

as stated $P_{required}$ is the instantaneous power required to fly the mission, P_i is the energy supplied to the i^{th} rotor and N is the total number of rotors in the UAV. In the current research, the following is assumed for the $P_{required}$:

$$P_{required} = P_{induced} + P_{parasite} \quad (29)$$

where $P_{induced}$ and $P_{parasite}$ are the induced and parasite power losses respectively.

2.9 Phase link

Each of the three phases in the trajectory is linked to the adjoining phases by a set of linkage conditions. These constraints force the position (along-track and altitude) and velocity (horizontal component and vertical component) to be continuous [23]. Hence, the problem is subject to phase link constraints on state variables (X) apart as follows:

$$X^{phase-1}(t_f^{phase-1}) = X^{phase}(t_0^{phase}) \quad (30)$$

2.10 Path Constraints

The path constraints are imposed on the multiphase optimal control problem based on the operational limitations of the UAV. The following path constraints are imposed on the multiphase problem for realistic trajectory generation:

$$\left(\frac{dh}{dt}\right)_{min}^{phase} \leq V_h \leq \left(\frac{dh}{dt}\right)_{max}^{phase} \quad (31)$$

$$V_{min} \leq V_x^{phase} \leq V_{max} \quad (32)$$

$$h^{phase} \leq 121.92 \text{ m (400 ft)} \quad (33)$$

2.11 Avoidance of Vortex Ring State in Descent

In order, to avoid Vortex Ring State (VRS) so that the UAV does not become uncontrollable during the descent phase the following additional path constraint is imposed on the descent phase of the problem [24]:

$$-0.28 \leq \frac{V \sin \alpha}{v_h} \leq 0 \quad (34)$$

where V is the true air speed, v_h is the induced speed in hover and α is the angle of attack of the tip path plane of the rotors.

3. NUMERICAL STUDY

The equations of motion of multicopter UAVs are continuous-time nonlinear differential equations and hence they are difficult to solve analytically. For this reason numerical-optimization technique has been used in the current research.

3.1 GPOPS-II

GPOPS-II is a commercially available general-purpose MATLAB software for solving multiphase optimal control problems using variable-order Gaussian quadrature collocation methods. The software employs a Legendre-Gauss-Radau quadrature orthogonal collocation method where the continuous-time optimal control problem is transcribed to a large sparse nonlinear programming problem (NLP) [23]. GPOPS-II has been used for solving the multiphase optimal control problems (maximum area coverage path and minimum energy path). The IPOPT has been used as the solver to solve the problems transcribed to NLP by GPOPS-II [25]. The numerical simulation was performed on a Macbook Pro with 2.8 GHz Intel Core i7 Processor.

3.2 DJI Phantom 4.0

DJI Phantom 4.0 with integrated Sentera (high precision multispectral single sensor camera) is considered for the simulation of trajectories. The horizontal field of view (FOV) of the multispectral camera is 60° , therefore the UAV footprint is as follows:

$$L = 2H \tan(30^\circ) \quad (35)$$

The path constraints for DJI phantom 4.0 are as follows:

$$V_h^{climb} \leq 6 \text{ m/s} \quad (36)$$

$$-4 \text{ m/s} \leq V_h^{descent} \quad (37)$$

$$V_x^{phase} \leq 20 \text{ m/s} \quad (38)$$

$$h^{phase} \leq 121.92 \text{ m (400 ft)} \quad (39)$$

$$-0.28 \leq \left(\frac{\sqrt{V_x^2 + V_h^2} \sin \alpha}{v_h} \right)^{descent} \leq 0 \quad (40)$$

The initial condition (IC) and final condition (FC) for the multi-phase optimal control problems are as shown in Table 1. The performance data required to compute Thrust and Drag are as shown in Table 2.

Table 1. Initial and Final Conditions

State Variable	IC	FC
Altitude	5 m	5 m
Along-track distance	0 m	Free
Ground Speed (GS)	0.1 m/s	0.1 m/s
Time	0 s	1200 s

Table 2. Performance Data

Variable	Value
Rotor Diameter	0.24 m
Mass	1.410 Kg
Equivalent Front Plate Area	0.012 m^2
Equivalent Top Plate Area	0.03 m^2

3.3 Simulation Results of Fixed Duration (20 Minutes) Flight Missions with Climb, Cruise and Descent Phases

The results of the following two fixed duration (20 mins) multi-phase (climb, cruise and descent) optimal control problems are discussed in this section:

- i) maximization of field area coverage.
- ii) minimization of energy consumed.

Finally, energy consumed (Kilo Joule (KJ)) by DJI Phantom 4.0 is plotted against various constant cruise ground speed missions, where each mission is of a fixed flight duration i.e. 20 mins.

A. Results of Maximum Field Area Coverage Mission

The numerical simulation for optimal field area coverage picked the cruise altitude of 121.92 m (400 ft) i.e. upper bound of sUAS flyable altitude and the cruise ground speed of 20 m/s i.e. the maximum cruise speed as shown in Table 3.

Table 3. Max Field Area Coverage

Altitude	Cruise GS	Range	Area Coverage
121.92 m	20 m/s	19205 m	2.016 km^2

B. Results of Minimum Energy Profiles for Various Constant Cruise Ground Speed Missions

The energy optimal vertical profiles and ground speeds for DJI Phantom 4.0 on various constant cruise ground speed missions (1, 3, 5, 7.5, 10, 12.5 and 15 m/s) are shown in Figure 5 and Figure 6. The numerical format of results from Figure 5 and Figure 6 are as shown in Table 4. From, Figure 5, Figure 6 and Table 4, it can be seen that higher the cruise ground speed greater is the corresponding range. Hence, from equation 23 and equation 24, this in turn implies higher area coverage for a given flight duration.

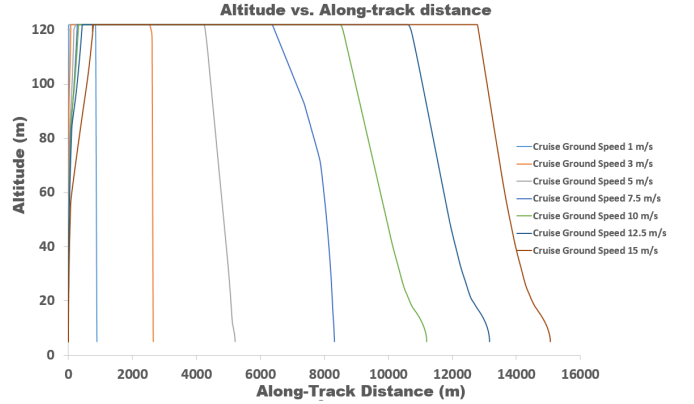


Figure 5. Min Energy: Vertical Profiles of DJI Phantom 4.0.

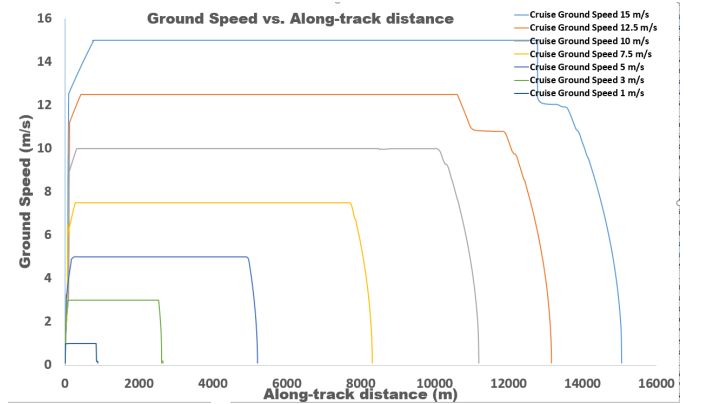


Figure 6. Min Energy: Ground Speeds of DJI Phantom 4.0.

Table 4. Min Energy: Cruise Ground Speed vs. Range

Cruise Ground Speed (m/s)	Range (m)
1	892
3	2652
5	5210
7.5	8315
10	11198
12.5	13163
15	15061

C. Results of Global Minimum Energy Consumption

The energy consumption (performance index) is calculated based on summation of induced power and parasite power, which is integrated over the total flight duration (20 mins) per equation 28 and equation 29. As stated before, the fixed duration (20 mins) flight with various constant cruise ground speeds (1, 3, 5, 7.5, 10, 12.5, 15 and 20 m/s) includes climb, cruise and descent phases. Based on the 3rd order polynomial fit of Figure 7 and the matlab function `fminbnd`, it is concluded that among the various constant cruise ground speed missions with a fixed flight duration (20 mins), the one with cruise ground speed of 12.089 m/s has the (global) minimum energy consumption.

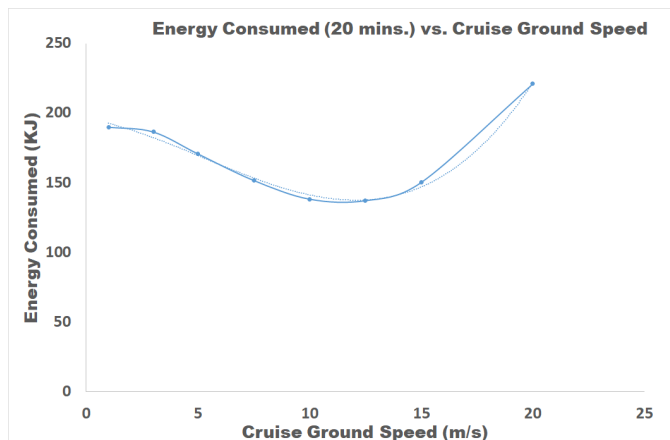


Figure 7. Energy Consumption vs. Cruise Ground Speed in 20 minutes flight

4. CONCLUSION

In this paper, the multi-phase optimal control problems are formulated for multirotor UAVs on an agricultural flight mission. The formulated fixed time multi-phase optimal control problems (maximum area coverage and minimum energy) were solved using a numerical method (pseudospectral) for a specific multirotor UAV i.e. DJI Phantom 4.0. The numerical results for maximization of field area coverage suggest that to maximize the performance index DJI Phantom 4.0 needs to fly fast (max speed) and fly high (max allowable altitude). However, to minimize energy consumption during the fixed duration flight, it needs to cruise at 12.089 m/s. The energy consumption curve of DJI Phantom 4.0 also suggests that multirotor UAVs are more suited for PA missions like detailed field surveying, spotting and close-in scouting instead of large field area coverage missions. This is because of sharp rise in

power required with increase in velocity beyond minimum energy speed. The proposed optimal control formulation can be applied to other multirotor UAVs like hexacopter and octocopter without the loss of generality.

REFERENCES

- [1] Ray, Deepak K., et al. "Yield trends are insufficient to double global crop production by 2050." *PloS one* 8.6 (2013): e66428.
- [2] Buhaug, Halvard, and Henrik Urdal. "An urbanization bomb? Population growth and social disorder in cities." *Global Environmental Change* 23.1 (2013): 1-10.
- [3] Shi, Yeyin, et al. "Unmanned aerial vehicles for high-throughput phenotyping and agronomic research." *PloS one* 11.7 (2016): e0159781.
- [4] Gebbers, Robin, and Viacheslav I. Adamchuk. "Precision agriculture and food security." *Science* 327.5967 (2010): 828-831.
- [5] Zhang, Chunhua, and John M. Kovacs. "The application of small unmanned aerial systems for precision agriculture: a review." *Precision agriculture* 13.6 (2012): 693-712.
- [6] Warren, Georgina, and Graciela Metternicht. "Agricultural Applications of High-Resolution Digital Multispectral Imagery." *Photogrammetric Engineering & Remote Sensing* 71.5 (2005): 595-602.
- [7] Zhang, Chunhua, Dan Walters, and John M. Kovacs. "Applications of low altitude remote sensing in agriculture upon farmers' requests: a case study in northeastern Ontario, Canada." *PloS one* 9.11 (2014): e112894.
- [8] Noriega, Alfonso, and Richard Anderson. "Linear-optimization-based path planning algorithm for an agricultural UAV." *AIAA Infotech@ Aerospace, AIAA SciTech Forum*. 2016.
- [9] Avellar, Gustavo SC, et al. "Multi-uav routing for area coverage and remote sensing with minimum time." *Sensors* 15.11 (2015): 27783-27803.
- [10] Pradeep, Priyank, et al. "Energy Efficient Arrival with RTA Constraint for Urban eVTOL Operations." to appear on *AIAA SciTech Forum* 2018.
- [11] Bottasso, Carlo L., et al. "Rotorcraft trajectory optimization with realizability considerations." *Journal of Aerospace Engineering* 18.3 (2005): 146-155.
- [12] Yomchinda, Thanan, Joseph F. Horn, and Jack W. Langelaan. "Flight path planning for descent phase helicopter autorotation." *AIAA Guidance, Navigation, and Control Conf.* 2011.
- [13] Johnson, Wayne. "Helicopter optimal descent and landing after power loss." (1977).
- [14] Hoffmann, Gabriel M., et al. "Quadrotor helicopter flight dynamics and control: Theory and experiment." *Proc. of the AIAA Guidance, Navigation, and Control Conference*. Vol. 2. 2007.
- [15] Morbidi, Fabio, Roel Cano, and David Lara. "Minimum-energy path generation for a quadrotor UAV." *Robotics and Automation (ICRA), 2016 IEEE International Conference on*. IEEE, 2016.
- [16] Heyson, Harry H. "A momentum analysis of helicopters and autogyros in inclined descent, with comments on operational restrictions." (1975).

- [17] Johnson, Wayne. Helicopter theory. Courier Corporation, 2012.
- [18] DeMoss, Joshua Andrew. "Drag measurements on an ellipsoidal body." (2007).
- [19] Xu, Anqi, Chatavut Viriyasuthee, and Ioannis Rekleitis. "Optimal complete terrain coverage using an unmanned aerial vehicle." Robotics and automation (ICRA), 2011 IEEE international conference on. IEEE, 2011.
- [20] Vrabel, Jim. "Multispectral imagery band sharpening study." Photogrammetric Engineering and Remote Sensing 62.9 (1996): 1075-1084.
- [21] Candiago, Sebastian, et al. "Evaluating multispectral images and vegetation indices for precision farming applications from UAV images." Remote Sensing 7.4 (2015): 4026-4047.
- [22] Neumann, Klaus J. "Trends for digital aerial mapping cameras." Int. Arch. Photogram. Rem. Sens. Spatial Info. Sci.(ISPRS) 28 (2008): 551-554.
- [23] Patterson, Michael A., and Anil V. Rao. "GPOPS-II: A MATLAB software for solving multiple-phase optimal control problems using hp-adaptive Gaussian quadrature collocation methods and sparse nonlinear programming." ACM Transactions on Mathematical Software (TOMS) 41.1 (2014): 1.
- [24] Chenglong, Li, et al. "A vortex-ring-state-avoiding descending control strategy for multi-rotor UAVs." Control Conference (CCC), 2015 34th Chinese. IEEE, 2015.
- [25] Wchter, Andreas, and Lorenz T. Biegler. "On the implementation of an interior-point filter line-search algorithm for large-scale nonlinear programming." Mathematical programming 106.1 (2006): 25-57.

BIOGRAPHY



Priyank Pradeep received Integrated degree (Bachelor of Technology and Master of Technology) in Aerospace Engineering from Indian Institute of Technology, Madras, India in 2006; Master of Science in Aeronautics and Astronautics from Purdue University, West Lafayette, IN, USA in 2013. He has over 8 years of experience in Avionics Industry working as Systems Engineer for Flight Management System (FMS) and Electronic Flight Bag (EFB). Currently, he is a Research Assistant with Iowa State University, Ames, IA, USA.



Sang Gyun Park is a research scientist at Optimal Synthesis Inc. He received the B.S. and M.S. degrees in Mechanical and Aerospace Engineering from Seoul National University, Korea in 2002 and 2004, respectively. He also received M.S in mathematics and Ph.D. degree in Aerospace Engineering from Georgia Institute of Technology in 2014. Before joining Georgia Tech, Dr. Park served as a research engineer for Hyundai Mobis and Hyundai Heavy Industries, Co. Ltd, Korea from 2004 to 2009. His research interests are control and optimization applications to various fields including avionics systems and the air traffic management.



Peng Wei is an assistant professor in Iowa State University Aerospace Engineering Department, with a courtesy appointment in Electrical and Computer Engineering Department. He is also an affiliated faculty member with the FAA Center of Excellence for General Aviation - PEGASAS, and the Human Computer Interaction graduate program at Virtual Reality Applications Center at ISU. He is leading the Intelligent Aerospace Systems Lab (IASL).

Dr. Wei received his undergraduate degree in Information Science and Control Theory from Tsinghua University in 2007, a master degree in Electrical and Computer Engineering from Stony Brook University in 2009, and a Ph.D. degree in Aerospace Engineering from Purdue University in 2013. Prior coming to ISU, Dr. Wei worked in American Airlines Operations Research Department on large-scale flight operation decision support and automation tools. His past research was featured in TIME Magazine cover story, Air Traffic Control Association Bulletin, CBSNews, NBC Today, Chicago Tribune, Seattle Times, Yahoo!, etc. Dr. Wei is a senior member of AIAA, and a member of IEEE, INFORMS, and AGIFORS.